ADVANCED OPTICAL MATERIALS
www.advopticalmat.de

Triangular Micro-Grating via Femtosecond Laser Direct Writing toward High-Performance Polarization-Sensitive Perovskite Photodetectors

Xiaoyu Tian, Ruonan Wang, Yalun Xu, Qianqian Lin, and Qiang Cao**

Thanks to attractive properties, such as defect tolerance, broad bandgap tunability, high quantum yields, and large absorption coefficient, perovskites have emerged as a star material in the past decade. Meanwhile, optical nano/microstructures made of perovskites offer a facile and efficient strategy to improve light-harvesting performance and sensitivity of polarization. However, there is no low-cost, high-accuracy, and reproducibility technique for large-scale fabrication of perovskite nano/microstructures. Here, femtosecond laser direct writing technique is introduced to fabricate $FAPbI_3$ perovskite micro-grating. Based on precise spatial and power control of femtosecond laser, micro-grating with different structure parameters (period and depth) can be processed and investigated. Triangular micro-grating of perovskite exhibits excellent emission properties (up to 67 times enhancement) owing to low reflectance and high absorption intensity. Strikingly, the outstanding performance of perovskite triangle grating photodetectors is obtained. The responsivity and detectivity reach 11.7 A W^{-1} and 7.8×10^{12} Jones, which are ≈3 and 12 times larger than the control devices; they also exhibit lower noise and decent polarization sensitivity. Taking the advantages of low cost, high accuracy, and reproducibility, the femtosecond laser direct writing technique endows perovskite materials with micro-photonic concept and remarkably enhances the devices' performance.

1. Introduction

Perovskite materials are fascinating materials with rich structural and chemical diversities (the crystal formula is ABX_3, A = $CH(NH_2)_2$ (FA), CH_3NH_3 (MA), Cs; B = Pb, Sn; X = Cl, Br, I). Owing to these outstanding optical and electrical properties, such as large refractive index,[1] strong nonlinear effects,[2] long carrier lifetime[3] and diffusion length,[4] low recombination rates,[5] broad bandgap tunability,[6] high absorption coefficient,[7] and quantum efficiency,[8] perovskites have demonstrated great advantages in many optoelectronic applications. Unfortunately, due to poor crystalline quality, scattering, and reflection in perovskite films, the performance of optoelectronic devices is largely limited.[9] Micro-nano optical structures provide an effective way to improve the utilization of incident light and enhance light absorption to obtain higher light conversion efficiency.

Especially, perovskite micro-nano grating, known as a common light dispersion component in optical systems, has attracted great attention and wide interest. Soci et al.[10] first demonstrated $MAPbI_3$ nanograting metasurfaces with structural tunable coloring via focused ion beam (FIB) milling and observed a three-fold increase of the luminescence yield, as well as a comparable reduction of luminescence decay time in comparison with unstructured perovskites films. Hu[11] and Makarov et al.[12] also observed eight-fold and ten-fold enhancement in photoluminescence (PL) intensity of perovskite rectangle nanograting by thermal nanoimprint, respectively. Meanwhile, many types of perovskite lasers with micro-nano grating have been experimentally demonstrated, for example, Whitworth et al.[13] combined solution-processed $MAPbI_3$ perovskite with UV nanoimprinted polymer gratings to fabricate distributed feedback (DFB) laser and achieved the lasing threshold as low as 4 μJ cm^{-2} under femtosecond (fs) pumping. Adachi et al.[14] produced stable quasi-2D perovskite lasers under continuous wave (CW) optical pumping in the air at room temperature by using a 2D gratings distributed-feedback cavity performed by electron beam lithography (EBL). Xiao et al.[15] demonstrated the perovskite vortex micro-lasers depended on $MAPbBr_3$ nano-gratings by

X. Tian
School of Mechanical Engineering
Wuhan Polytechnic University
Wuhan 430048, China
R. Wang, Q. Cao
The Institute of Technological Sciences
Wuhan University
Wuhan 430072, China
E-mail: caoqiang@whu.edu.cn
Y. Xu, Q. Lin
School of Physics and Technology
Wuhan University
Wuhan 430072, China
E-mail: q.lin@whu.edu.cn
Y. Xu, Q. Lin
Suzhou Institute of Wuhan University
Suzhou 255123, China
The ORCID identification number(s) for the author(s) of this article can be found under https://doi.org/10.1002/adom.202200856.

DOI: 10.1002/adom.202200856

EBL and inductively coupled plasma etching (ICPE). However, perovskite is extremely sensitive to light, ion/electron beam,[16] polar organic solvents, and high temperatures above 180 °C,[17] which makes it incompatible and impractical for lithographic techniques with an ion beam, electron beam, solution-based or dry etching approaches. So, it is necessary to find a precise, controllable, and less damaged fabrication method to fabricate perovskite micro-nano grating.

By the manipulation of microstructure, perovskite nan-micro grating can enhance the light-harvesting of solar cells and photodetectors, for example, Song et al.[18] introduced a large area grating structure into the perovskite-active layer of a solar cell by utilizing commercial optical discs (CD-R and DVD-R) and obtained high power conversion efficiency and photocurrent density. Li et al.[19] employed a double grating design on a commercial compact disk (CD) as the hard mold to increase the photocurrent in perovskite solar cells. Qi et al.[20] achieved high-performance photodetectors (responsivity of 7.66 A W^{-1} and detectivity of $\approx 10^{12}$ Jones) using $CsPbBr_3$ perovskite micro–nanowire array by a sequential vapor deposition and growth method. Li et al.[21] used 1D nanograting bonded porous 2D photonic crystal using a DVD master and 2D crystalline colloidal arrays template to fabricate a high-performance polarization-sensitive perovskite photodetector. Owing to the advantages of facile, low cost, less damage, high reproducibility, and batch manufacturing, nanoimprinting has attracted more attention for the fabrication of perovskite grating microstructures. However, this CD/DVD imprinting approach depends on as-prepared templates and lacks diversity.

Despite the continuous success, there are still several challenges remaining for the application of perovskite micro-nano grating, including i) The preparation of perovskite film: perovskite film is usually prepared by solution processes, which only achieves a maximal film thickness of ≈700 nm due to the limited solubility and viscosity; ii) The fabrication of perovskite micro-grating: it is still challenging to realize low damage, direct patterned, precise, and controllable manufacturing technology to fabricate specially shaped perovskite micro grating with high crystal quality and good optical properties. iii) The optical properties of perovskite micro grating: while many researches have been undertaken on fabricating different perovskite microstructures and applied to different photoelectric devices, few works focused on the optical properties and physical mechanism of different perovskite grating structures systematically.

In this work, we use fs laser direct writing to obtain perovskite triangular micro-grating based on thick formamidinium lead iodide ($FAPbI_3$) films (≈6.12 µm) fabricated by thermal co-evaporation and find multifold emission enhancement (up to 67-fold) in $FAPbI_3$ perovskite triangular micro-grating. Then, we systematically investigate the optical properties of different structures of perovskite grating and find that emission enhancement is greatly dependent on the grating period and depth. At last, perovskite photodetectors based on $FAPbI_3$ perovskite triangular grating with the largest emission enhancement were fabricated. Encouragingly, triangular grating photodetectors have better optoelectronic performance, such as high responsivity, detectivity, low noise, and high sensitive polarization, compared with unpatterned perovskite film photodetectors. Fs laser direct writing with facile, maskless, desirable controllability, and reproducibility is a promising technology to combine perovskite material and microstructure to explore the interaction of light and matter. Perovskite triangular gratings are helpful for applications requiring emission enhancement, antireflection, and polarization selection, and can be envisioned as a route for further implementation of the new generation of optoelectronic devices.

2. Results and Discussion

2.1. Fabrication and Characterization of $FAPbI_3$ Perovskite Triangular Grating Microstructure

The schematic illustrations of a direct triangular grating microstructure method are shown in **Figure 1**a–c. First, a solid-state $FAPbI_3$ film with a thickness of 6.12 µm is prepared by thermal co-evaporation on the silicon substrates (300 nm Si/SiO_2) (Figure 1a) and this method is reported in our previous works.[22,23] The sectional view scanning electron microscope (SEM) picture of $FAPbI_3$ film is shown in Figure S1a, Supporting Information. Specially, we evaporated a thin layer of CsI at about 10 nm at first to improve the perovskite film's stability. Second, $FAPbI_3$ film is put on a hotplate for gradient annealed from 60 to 120 °C (10 min) and 140 °C (2 h) in a glovebox filled with N_2 to promote the crystallization (Figure 1b). It can be found that the color of perovskite films changed from brown to black, indicating the desired pure α-phase was obtained. Next, we use a femtosecond laser to "write" directly with the triangular grating microstructure on the 6.12 µm $FAPbI_3$ perovskite films (Figure 1c). The top view SEM picture of the $FAPbI_3$ perovskite triangular grating microstructure is shown in Figure S1b, Supporting Information. The optical microscopy image and 3D laser scanning confocal microscope image of a big area (2 mm × 1.5 mm) $FAPbI_3$ perovskite triangular grating are shown in Figure S1c,d, Supporting Information. Finally, perovskite triangular grating microstructure can effectively improve light absorption through light scattering (Figure 1d).

In this work, we used fs laser (514 nm, 190 fs, 200 kHz) to draw a line array of about 100 µm length in $FAPbI_3$ perovskite film with different attenuation power, the SEM image is shown in Figure S2a, Supporting Information. As Figure S2b, Supporting Information, shows, the width and depth of lines are highly dependent on laser power. The linear relationships are shown in Figure S2c,d, Supporting Information. Notably, we can obtain triangular grating with specific parameters, for example, to get the ≈800 nm depth of triangular grating, the laser power (P) should be ≈142 mW, and width (W) is ≈9.2 µm.

In this method, a triangular grating with a depth of ≈800 nm and a period of ≈10 µm can be obtained and the SEM and EDS are shown in Figure 1e,f. Uniform grating structure in perovskite film can be found and there are no visible collateral damages around the grating. As seen in the enlarged SEM image, the perovskite grain size increases in the valley where the laser scanned. This result indicates that fs laser may help grain growth with better crystallinity, which is important for carrier transport, photoluminescence lifetime, and solar cell power conversion efficiency.[24,25] Besides, the EDS spectra (Figure 1f) show that the perovskite grating structure is composed mainly

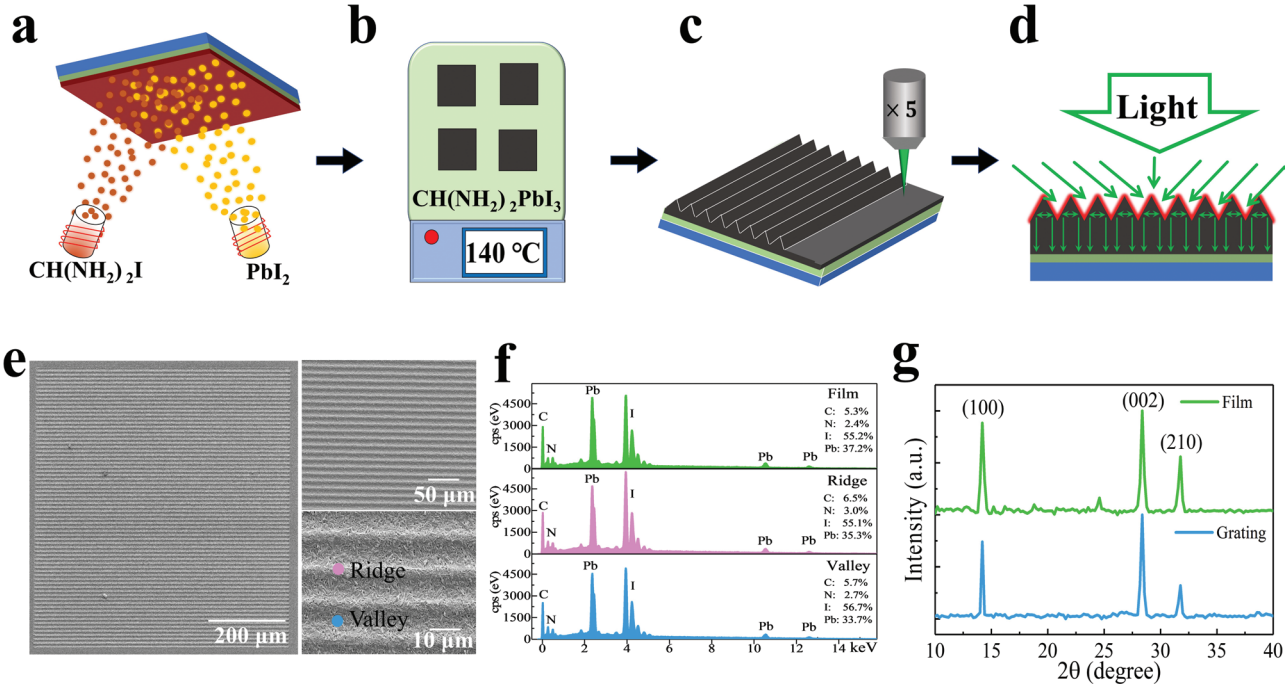

Figure 1. a–d) Schematic illustration of the fabrication processes of $CH(NH_2)_2PbI_3$ ($FAPbI_3$) film, annealed condition, $FAPbI_3$ grating microstructure, and 532 nm laser-induced light moment in $FAPbI_3$ grating microstructure. e) SEM image and f) EDS spectra of $FAPbI_3$ perovskite grating structure with periods $\Lambda = 10$ μm. g) XRD patterns of perovskite thin films and grating.

of the C, N, I, and Pb elements and corresponding element ratio (I/Pb) in a different area (Film, Ridge, and Valley) is close to 1.5 in Table S1, Supporting Information. This result is consistent well with the stoichiometric ratio of the $FAPbI_3$ phase, indicating fs laser can avoid thermal accumulation effects and result in low damage to perovskite materials. On the other hand, during fs laser irradiation, photons are mainly absorbed by electrons, and the subsequent energy transfer from electrons to ions is in the picosecond order. Thus, lattice motion is negligible during the duration of the fs pulse, with fs photon-electron interactions dominating the entire irradiation process.[26,27] Figure 1g shows the X-ray diffraction (XRD) patterns of perovskite film and grating, which exhibits clean diffraction peaks at approximately 14°, 28°, and 32° of the α-phase $FAPbI_3$ perovskite crystal structure, corresponding to the diffraction of (100), (002), and (210) planes, respectively.[28]

2.2. Optoelectronic Properties of $FAPbI_3$ Perovskite Grating Microstructure

Next, we fabricate $FAPbI_3$ perovskite gratings with different depths by changing the laser power and fabricate different periods by changing the distance between two lines to study the optical properties of different $FAPbI_3$ perovskite grating microstructure.

To fabricate different periods of $FAPbI_3$ perovskite grating, we keep the laser power constant (200 mW, 70%) and gradually reduce the period from 30 to 9 μm. Since the femtosecond laser is a Gaussian beam, the bottom of the grating has a triangular profile, the SEM pictures of typical gratings (Λ = 30, 20, 15, 14, 13, 12, and 10 μm) are shown in **Figure 2**a–h. It can be clearly seen that the gratings obtain a uniform depth (about 800 nm), which fully indicates the stable manufacturing process of the fs laser. Interestingly, when the grating period is Λ = 30 μm, the laser scanning edge is relatively flat (Figure 2a). Once the grating period is $\Lambda \leq 20$ μm, obvious bulges (about 400 nm) will appear on both sides of the laser scanning (Figure 2b–h). As the grating period gradually decreases, the bulges overlap perfectly to form a triangle, as shown in Figure 2g,h. The 3D morphology of representative $FAPbI_3$ perovskite grating structure (Λ = 15, 13, 12, 10, and 9 μm) by laser confocal microscope shows the favorable formation process of the triangular grating shown in Figure 2i–m.

$FAPbI_3$ perovskite grating structures demonstrate highly efficient PL at the wavelength of 790 nm and it is possible to enhance PL via excitation of optical resonance modes in the emitting material. To understand the optical properties of laser irradiation on the perovskite grating, the PL spectra of different perovskite triangular grating microstructures under 532 nm continuous laser photoexcitation are investigated.

PL spectra at different attenuation powers of fs laser (50%, 55%, 60%, 65%, and 70%) are shown in **Figure 3**a. We find that PL intensity increases as grating depth and the fs laser power of 200 mW (70%) can obtain the highest PL intensity. Next, laser attenuation power is maintained constant (200 mW, 70%) and perovskite grating periods are changed from 9 to 13 μm. PL spectra at different grating periods (Λ = 9, 9.5, 10, 11, 12, and 13 μm) are shown in Figure 3b. We can find that PL intensity decreases as the grating period increases. The $FAPbI_3$ perovskite grating with line width equal to the period (P = 200 mW, 70%; W = 8.8 μm; Λ = 9 μm) exhibited the best spontaneous emission properties up to 67 times enhancement.

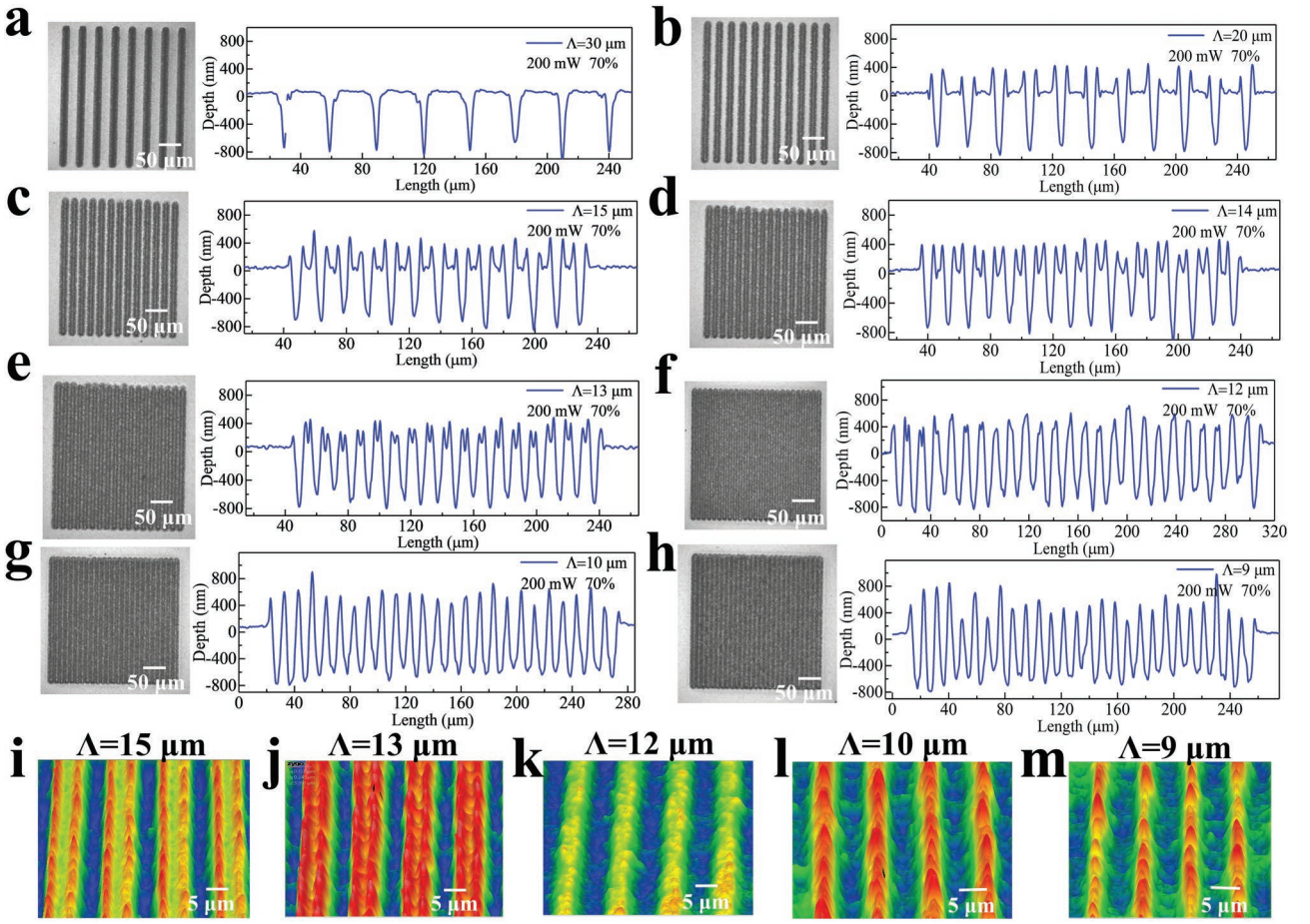

Figure 2. Optical microscopy images and corresponding cross-section height diagram of $FAPbI_3$ perovskite grating structure with different periods: a) Λ = 30 μm, b) 20 μm, c) 15 μm, d) 14 μm, e) 13 μm, f) 12 μm, g) 10 μm, and h) 9 μm. 3D morphology of representative $FAPbI_3$ perovskite grating structure by laser confocal microscope: i) Λ = 15 μm, j) 13 μm, k) 12 μm, l) 10 μm, and m) 9 μm.

To investigate the PL enhancement factors deeply, absorption and reflection spectra of gratings with line width equal to the period (denoted as "triangular grating") structures with two periods (Λ = 9, and 10 μm) and perovskite film without patterns are tested. $FAPbI_3$ perovskite demonstrates high absorption intensity below 790 nm as shown in Figure 3c, this is because that perovskite film is too thick (≈6.12 μm) to exceed the limit of the spectrometer. Especially, when the wavelength is >790 nm, the absorption spectra between perovskite film and triangular grating structures are different due to surface scattering. Nevertheless, the reflectance intensities of perovskite gratings were greatly attenuated, compared with the unpatterned samples as shown in Figure 3d. Unlike the control perovskite films are plane, causing specular reflection and energy loss, the PL enhancement of the $FAPbI_3$ perovskite triangular grating micro-pattern can be partially explained by the increase of light absorption due to the enhanced light trapping. However, the increase of absorbed photons was not able to explain the superb PL gain, and additional analysis of the internal changes of the material is presented.

We explore the carrier dynamics of perovskite triangular grating, transient absorption (TA) spectra of perovskite film and triangular grating are obtained in Figures S3a and S3c, Supporting Information, respectively. TA spectra of $FAPbI_3$ perovskite films have three main features: photo-induced absorption (PA) at 750 and 850 nm, and ground state bleach (GSB) at 790 nm. We can observe that the PA1 signal of triangular grating microstructures increases compared with perovskite plane film. This phenomenon may originate from the effect of resonances (e.g., Purcell factor) of triangular grating microstructures and increasing perovskite's grain size via fs laser direct writing. The Purcell factor of triangular grating microstructure for emitting dipoles in a resonator with a higher local density of states (LDOS) leads to an acceleration of spontaneous emission.[29–32]

On the other hand, we also observed that the GSB and PA2 signals decreased compared with perovskite plane film, which may be due to the high defect density of perovskite grating by fs laser direct writing, resulting in a faster recovery of the GSB signal.[33] For quantitative interpretation of the GSB signal, GSB recovery signals are recorded for analyzing the carrier relaxation dynamics. The signals are fitted with the biexponential function $y = y_0 + A_1\exp(-x/\tau_1) + A_2\exp(-x/\tau_2)$ and the fast component τ_1 is attributed to charge carrier recombination at the interface, whereas τ_2 is attributed to band-to-band recombination in the interior of the grain. The kinetic fitting

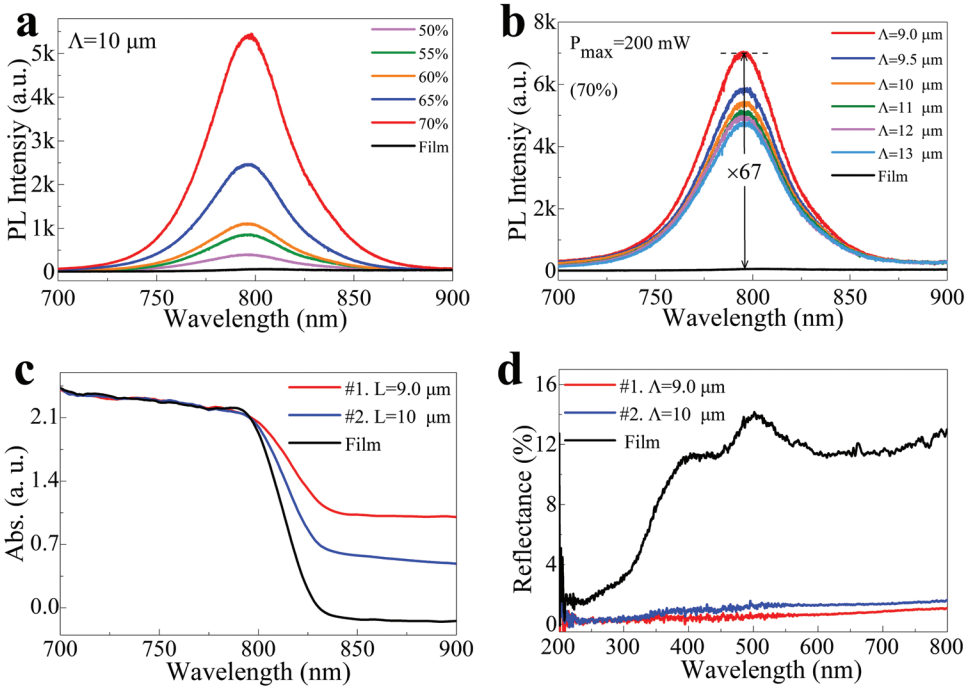

Figure 3. Optical properties. a) PL spectrum of the $CH(NH_2)_2PbI_3$ ($FAPbI_3$) perovskite film (black) and grating structures (Λ = 10 μm) with different fs laser power (P_{max} = 200 mW, 50%, 55%, 60%, 65%, and 70%). b) PL spectrum of the $CH(NH_2)_2PbI_3$ ($FAPbI_3$) perovskite film (black) and different grating structures (Λ = 9.0, 9.5, 10, 11, 12, and 13 μm) in the same fs laser power (P_{max} = 200 mW, 70%). c) Absorption and d) reflection spectra of $FAPbI_3$ perovskite film (black), the grating structures with two periods of Λ = 9 μm (red) and 10 μm (blue).

results are illustrated in Figures S3b and S3d, Supporting Information, respectively. The fitting result of perovskite film indicates two characteristic time constants, $\tau_1 \approx 3890$ ps and $\tau_2 \approx 3891$ ps, while two characteristic time constants τ_1 and τ_2 were decreased to 27 and 693 ps of perovskite triangular gratings structures, respectively. The results indicate that defects in the interface and internal of perovskite grains hinder the general excitation, recombination, and transfer behaviors in the carrier relaxation dynamics.

2.3. Device Performance of $FAPbI_3$ Perovskite Grating Based Photodetectors

Highly sensitive photodetector-based different structures arouse the wide interest of researchers.[34–38] In this work, perovskite photodetectors based on triangular grating structured perovskite films (Λ = 9.0 μm, P_{max} = 200 mW, 70%) are constructed to study the effect of grating on device performance. The device was completed by thermal evaporation of a 60 nm metal electrode (Au) on triangular grating structured perovskite films. The channel length of the two metal electrodes was 0.1 mm, defined by a shadow mask during evaporation.

Under the bias from −5 to 5 V, the power-dependent logarithmic current–voltage (I–V) curves of the triangular grating device and film device are shown in **Figure 4**a and Figure S4a, Supporting Information, respectively. The good symmetrical linear relationship of the I–V curve indicates the good ohmic contact between the Au electrode and perovskite triangular grating. Additionally, as the incident light intensity increased, the photocurrent of the device was greatly increased at the same bias value because more carriers were excited and separated. Differently, the photocurrent of the triangular grating device can reach 290 nA under the illumination intensity of 30 mW cm^{-2} at the 5 V bias, which is almost five times higher than that of the film device (62 nA). The higher photocurrent of the grating device originates from more photon absorption induced by more carrier generation, which further demonstrates the enhanced light-harvesting ability of the perovskite triangular grating microstructure. Besides, the improved crystallinity and larger grain sizes of perovskite film caused by the fs laser direct writing process also make great contributions to the higher photocurrent.

Moreover, time-dependent current curves (I–t) of perovskite triangular grating and film photodetector under the various illumination intensity from 0.06 to 30 mA cm^{-2} at 5 V bias are shown in Figure 4b and Figure S4b, Supporting Information, respectively. High repeatability of perovskite triangular grating and film photodetector was demonstrated with repeated light on–off cycles. The relevant light on/off ratio (I_{ph}/I_d, I_{ph} is photocurrent, I_d is dark current) of perovskite triangular grating photodetector can reach 1.01×10^3 (5 V, 30 mW cm^{-2}), which is almost six times higher than perovskite film photodetector (0.18×10^3) in Table S2, Supporting Information. These enhanced on/off ratios (I_{ph}/I_d) indicate that perovskite triangular grating photodetector has better optoelectronic properties than perovskite film photodetector based on enhanced light-harvesting and higher crystallinity.

Responsivity (R) and detectivity (D^*) are also important parameters for photodetectors, representing the efficiency of

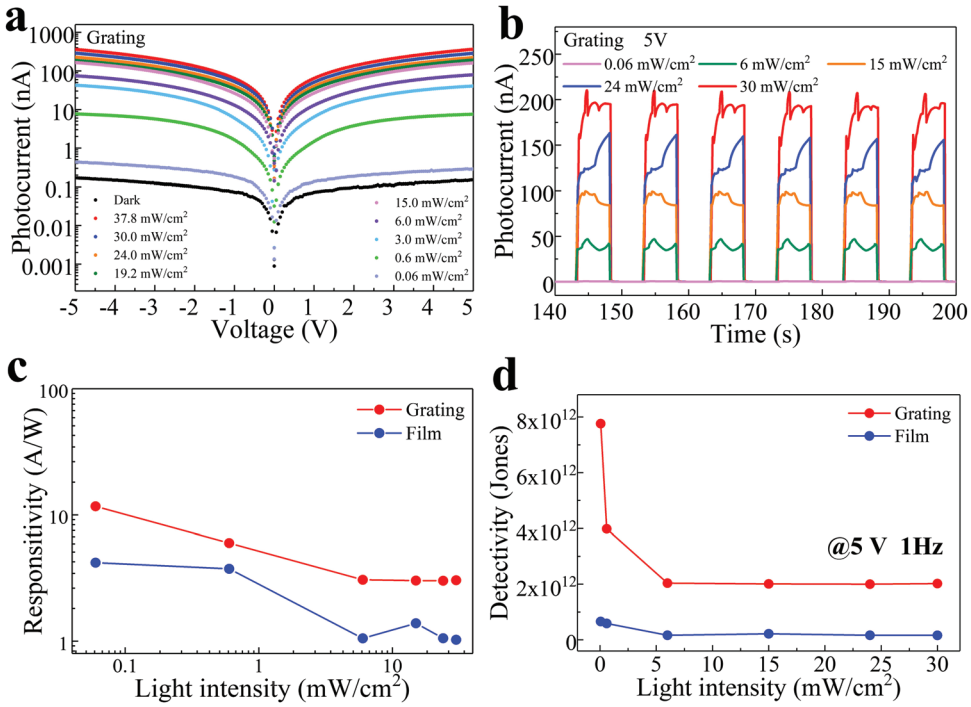

Figure 4. Optoelectronic properties of perovskite triangular grating photodetector. a) *I–V* curves and b) *I–t* curves under various light intensities of 532 nm laser from 0.06 to 30 mW cm^{-2}. c) Responsivity and d) detectivity of perovskite triangular grating photodetector (red) and film photodetector (blue) at 5 V bias under the light intensity from 0.06 to 30 mW cm^{-2}.

photodetectors. R is the photocurrent generated per unit area of light intensity, which is defined as:[39]

$$R = \frac{I_{ph} - I_d}{P \times S} \tag{1}$$

where P is incident light intensity and S is the effective incident area. In our experiment, the area of perovskite triangular grating (S) is 0.2 mm^2 (length: 2 mm, width: 0.1 mm). Because photocurrent is saturated with increasing incident light intensity, the responsivity of perovskite triangular grating and film photodetector decreases as shown in Figure 4c.

Detectivity (D^*) is commonly used to characterize the sensitivity of a photodetector. There are three factors that affect D^*, shot noise, thermal fluctuation noise, and Johnson noise. When the main contribution to D^* is shot noise from dark current, the D^* can be defined as:[40,41]

$$D^* = \frac{R\sqrt{SB}}{I_{noise}} \tag{2}$$

where B is the testing bandwidth and I_{noise} is the measured noise current. The detectivity as a function of illumination intensity of perovskite triangular grating and film photodetector displays the same trend as responsivity as shown in Figure 4d. Especially, the responsivity (R) and detectivity (D^*) of perovskite triangular grating photodetector are calculated to be 11.7 A W^{-1} and 7.8 × 10^{12} Jones, which are ≈3 and 12 times higher than perovskite film photodetectors (4.2 A W^{-1}, 6.5 × 10^{11} Jones) under the light intensity of 0.06 mW cm^{-2}. The corresponding value (dark current I_d and photocurrent I_{ph}) of perovskite triangular grating and film photodetector at 5 V bias under the illumination intensity from 6 to 30 mW cm^{-2} are shown in Table S2, Supporting Information. Furthermore, the responsivity and detectivity of the perovskite triangular grating photodetector are comparable to or higher than those of the reported Au-perovskite-Au photodetector (Table S3, Supporting Information). These results prove that perovskite triangular grating fabricated by fs laser direct writing has better optoelectronic performance than perovskite film photodetector.

The corresponding noise current spectra of two types of photodetectors in dark at different biases (0, 1, 2, and 5 V) are presented in Figure S5a,b, Supporting Information. They all have low noise benefiting from less device leakage, which is consistent with the previous report[42] about thick-junction perovskite photodetectors. Obviously, the photodetector based on perovskite triangle grating exhibited lower noise (≈1 × 10^{-29} A^2 Hz^{-1}) at a 5 V bias of 5 Hz as shown in Figure S5c, Supporting Information, than perovskite film (≈3.2 × 10^{-29} A^2 Hz^{-1}). To illustrate the issue more convincingly, we calculate the average noise density from 0 bias to 5 V and the results are shown in Figure S5d, Supporting Information. Intriguingly, the noise of photodetectors is increased remarkably with bias and the perovskite triangle grating photodetector exhibited lower noise than the unpatterned perovskite film photodetector under bias.

Furthermore, the perovskite triangular grating forms an anisotropic and very regular periodic surface structure, which can produce a polarization effect for realizing polarized light detection.[43,44] As illustrated in **Figure 5**a, the perovskite triangular grating photodetector is illuminated by linearly polarized light with changing polarization directions. The *I–V* curves of perovskite film and triangular grating photodetector on

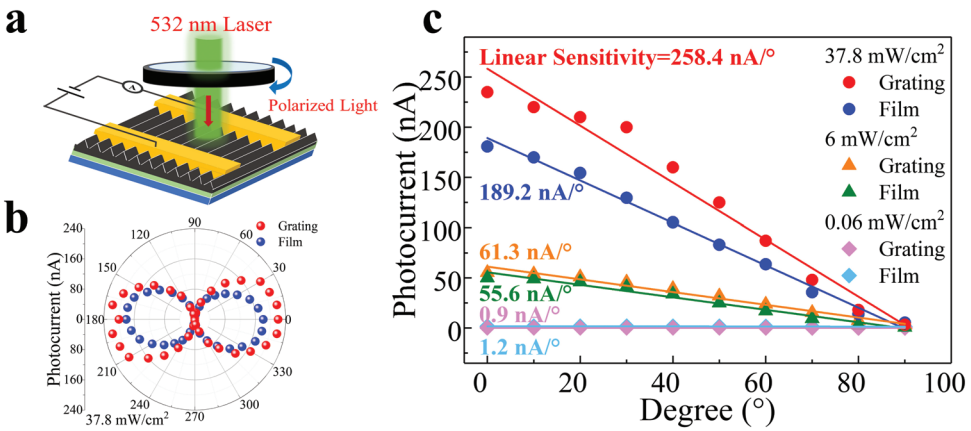

Figure 5. Polarization sensitivity of perovskite triangular grating photodetector. a) Illustration of polarization-sensitive photodetection of perovskite grating photodetector. b) Photocurrent dependence of perovskite triangular grating and film photodetector on 0°–360° polarization angle at 5 V bias in 37.8 mW cm^{-2} illumination intensity. c) Linear sensitivity of perovskite triangular grating and film photodetector in various illumination intensities (0.06, 6, and 37.8 mW cm^{-2}) on 0–90° polarization angle.

0°–180° polarization angle is shown in Figure S6, Supporting Information. Photocurrent dependence on polarization angle (Figure 5b) shows that the highest and smallest photocurrent appears at 0° and 90° polarization direction, respectively. Linear polarization (P) is the crucial figure of merit for the evaluation of the performance of polarized photodetection. Linear polarization is normally defined as:

$$P = \frac{I_{max} - I_{min}}{I_{max} + I_{min}} \quad (3)$$

where I_{max} is the testing highest photocurrent and I_{min} is the smallest photocurrent, which appears at 0° and 90° polarization direction at the period (0°–90°), respectively. The linear polarization (P) of the perovskite triangular grating photodetector is calculated to be 0.97 under the light intensity of 37.8 mW cm^{-2}. This result indicates that unidirectional perovskite triangular grating arrays render polarized light detection. To illuminate the polarization detection performance clearly, we define linear sensitivity as the ratio of photocurrent to a degree. Figure 5c displays the linear sensitivity of perovskite triangular grating and film photodetector in various illumination intensity (0.06, 6, and 37.8 mW cm^{-2}). There is no significant difference between perovskite triangular grating and film photodetector in low illumination intensity of 0.06 mW cm^{-2}, once increased illumination intensity to 37.8 mW cm^{-2}, perovskite triangular grating photodetector has better linear sensitivity (258.4 nA/°) than perovskite film photodetector (189.2 nA/°). That is because the light-trapping capacity of the $FAPbI_3$ perovskite triangle grating microform increases as the light intensity increases, ultimately leading to an increase in photocurrent.[45–49] The periodic microstructure with anisotropic dielectric function enables anisotropic optical absorption, yielding anisotropic photocurrents with a rotation of linear polarization. Perovskite triangular grating suggests excellent performance for linearly polarized light detection due to the strictly aligned gratings and the high light-trapping capacity. It demonstrates the potential application in the optoelectronic imaging system.

3. Conclusion

In summary, we show a novel approach by thermal co-evaporation and femtosecond laser direct writing to fabricate large-scale $FAPbI_3$ perovskite triangular grating microstructure and found that perovskite triangular grating microstructure for near-IR ranges with significantly enhanced PL properties (enhanced up to 67 times under 532 nm laser photoexcitation). We studied optical properties at first, indicating that the enhancement is achieved via increased absorption. Then through exploring the carrier dynamics, we found that the decrease of GSB and PA2 signal in transient absorption spectra, due to the high defect density in the perovskite grating by fs laser direct writing, which induced a faster recovery of the GSB signal. Next, we investigated the optoelectronic properties of $FAPbI_3$ perovskite triangular grating-based photodetectors, which have higher responsivity and detectivity than unpatterned perovskite film photodetectors. Furthermore, perovskite triangular grating photodetector was demonstrated to have better polarization detection performance to develop a polarization-sensitive photodetector. Our results show that $FAPbI_3$ perovskites are unique materials enabling high-accuracy and reproducibility technique (fs laser direct writing) for large-scale fabrication of microstructures with a high refractive index, which can be used to develop optimized planar microdevices for highly efficient photodetectors, lasers, LEDs, and amplifiers.

Supporting Information

Supporting Information is available from the Wiley Online Library or from the author.

Acknowledgements

This work was financially supported by the Strategic Priority Research Program of the Chinese Academy of Sciences (Grant No. XDA25040201), the National Natural Science Foundation of China (Grant No. 61875154), the Natural Science Foundation of Jiangsu Province, China (Grant

No. BK20190214), the National Key R&D Program of China (Grant No. 2020YFB2008800), and Wuhan Science and Technology Bureau (2022010801010108).

Conflict of Interest

The authors declare no conflict of interest.

Data Availability Statement

The data that support the findings of this study are available from the corresponding author upon reasonable request.

Keywords

femtosecond laser direct writing, micro-grating, perovskite photodetectors, thermal co-evaporation

Received: April 12, 2022
Revised: June 7, 2022
Published online:

[1] P. Löper, M. Stuckelberger, B. Niesen, J. Werner, M. Filipič, S. J. Moon, J. H. Yum, M. Topič, S. De Wolf, C. Ballif, *J. Phys. Chem. Lett.* **2015**, *6*, 66.
[2] T.-C. Wei, S. Mokkapati, T.-Y. Li, C.-H. Lin, G.-R. Lin, C. Jagadish, J.-H. He, *Adv. Funct. Mater.* **2018**, *28*, 1707175.
[3] J. Tong, Z. Song, D. Hoe, X. Chen, C. Chen, A. F. Palmstrom, P. F. Ndione, M. O. Reese, S. P. Dunfield, O. G. Reid, J. Liu, F. Zhang, S. P. Harvey, Z. Li, S. T. Christensen, G. Teeter, D. Zhao, M. M. Al-Jassim, M. F. A. M. van Hest, M. C. Beard, S. E. Shaheen, J. J. Berry, Y. Yan, K. Zhu, *Science* **2019**, *364*, 475.
[4] S. D. Stranks, G. E. Eperon, G. Grancini, C. Menelaou, M. J. P. Alcocer, T. Leijtens, L. M. Herz, A. Petrozza, H. J. Snaith, *Science* **2013**, *342*, 341.
[5] C. M. Wolff, P. Caprioglio, M. Stolterfoht, D. Neher, *Adv. Mater.* **2019**, *31*, 1902762.
[6] G. Xing, N. Mathews, S. S. Lim, N. Yantara, X. Liu, D. Sabba, M. Grätzel, S. Mhaisalkar, T. C. Sum, *Nat. Mater.* **2014**, *13*, 476.
[7] J. De Roo, M. Ibáñez, P. Geiregat, G. Nedelcu, W. Walravens, J. Maes, J. C. Martins, I. Van Driessche, M. V. Kovalenko, Z. Hens, *ACS Nano* **2016**, *10*, 2071.
[8] K. Lin, J. Xing, L. N. Quan, F. de Arquer, P. García, X. Gong, J. Lu, L. Xie, W. Zhao, D. Zhang, C. Yan, W. Li, X. Liu, Y. Lu, J. Kirman, E. H. Sargent, Q. Xiong, Z. Wei, *Nature* **2018**, *562*, 245.
[9] J. Wei, R. Xu, Y. Li, C. Li, J. Chen, X. Zhao, Z. Xie, C. Lee, W. Zhang, J. Tang, *Adv. Energy Mater.* **2017**, *7*, 1700492.
[10] B. Gholipour, G. Adamo, D. Cortecchia, H. N. S. Krishnamoorthy, M. D. Birowosuto, N. I. Zheludev, C. Soci, *Adv. Mater.* **2017**, *29*, 1604268.
[11] H. Wang, S.-C. Liu, B. Balachandran, J. Moon, R. Haroldson, Z. Li, A. Ishteev, Q. Gu, W. Zhou, A. Zakhidov, W. Hu, *Opt. Express* **2017**, *25*, 1162.
[12] S. V. Makarov, V. Milichko, E. V. Ushakova, M. Omelyanovich, A. Cerdan Pasaran, R. Haroldson, B. Balachandran, H. Wang, W. Hu, Y. S. Kivshar, A. A. Zakhidov, *ACS Photonics* **2017**, *4*, 728.
[13] G. L. Whitworth, J. R. Harwell, D. N. Miller, G. J. Hedley, W. Zhang, H. J. Snaith, G. A. Turnbull, I. D. W. Samuel, *Opt. Express* **2016**, *24*, 23677.
[14] C. Qin, A. S. D. Sandanayaka, C. Zhao, T. Matsushima, D. Zhang, T. Fujihara, C. Adachi, *Nature* **2020**, *585*, 53.
[15] W. Sun, Y. Liu, G. Qu, Y. Fan, W. Dai, Y. Wang, Q. Song, J. Han, S. Xiao, *Nat. Commun.* **2020**, *11*, 4862.
[16] N. Klein-Kedem, D. Cahen, G. Hodes, *Acc. Chem. Res.* **2016**, *49*, 347.
[17] J. S. Manser, M. I. Saidaminov, J. A. Christians, O. M. Bakr, P. V. Kamat, *Acc. Chem. Res.* **2016**, *49*, 330.
[18] Y. Wang, P. Wang, X. Zhou, C. Li, H. Li, X. Hu, F. Li, X. Liu, M. Li, Y. Song, *Adv. Energy Mater.* **2018**, *8*, 1702960.
[19] K. Deng, Z. Liu, M. Wang, L. Li, *Adv. Funct. Mater.* **2019**, *29*, 1900830.
[20] G. Tong, M. Jiang, d. y. Son, L. Ono, Y. Qi, *Adv. Funct. Mater.* **2020**, *30*, 2002526.
[21] Y. Zhan, Y. Wang, Q. Cheng, C. Li, K. Li, H. Li, J. Peng, B. Lu, Y. Wang, Y. Song, L. Jiang, M. Li, *Angew. Chem., Int. Ed.* **2019**, *58*, 16456.
[22] X. Tian, Y. Xu, H. Zhao, X. Qin, Y. Nie, W. Li, S. Liu, Q. Lin, Q. Cao, *J. Mater. Chem. C* **2020**, *8*, 7314.
[23] X. Tian, L. Wang, W. Li, Q. Lin, Q. Cao, *ACS Appl. Mater. Interfaces* **2021**, *13*, 16952.
[24] D. W. De Quilettes, S. M. Vorpahl, S. D. Stranks, H. Nagaoka, G. E. Eperon, M. E. Ziffer, H. J. Snaith, D. S. Ginger, *Science* **2015**, *348*, 683.
[25] J. Xiao, Y. Yang, X. Xu, J. Shi, L. Zhu, S. Lv, H. Wu, Y. Luo, D. Li, Q. Meng, *J. Mater. Chem. A* **2015**, *3*, 5289.
[26] L. Jiang, A.-D. Wang, B. Li, T.-H. Cui, Y.-F. Lu, *Light: Sci. Appl.* **2018**, *7*, 17134.
[27] N. Zhang, X. Zhu, J. Yang, X. Wang, M. Wang, *Phys. Rev. Lett.* **2007**, *99*, 167602.
[28] F. Cordero, F. Craciun, F. Trequattrini, A. Generosi, B. Paci, A. M. Paoletti, G. Pennesi, *J. Phys. Chem. Lett.* **2019**, *10*, 2463.
[29] M. Boroditsky, R. Vrijen, R. Coccioli, R. Bhat, E. Yablonovitch, *J. Light. Technol.* **1999**, *17*, 2096.
[30] E. Y. Tiguntseva, G. P. Zograf, F. E. Komissarenko, D. A. Zuev, A. A. Zakhidov, S. V. Makarov, Y. S. Kivshar, *Nano Lett.* **2018**, *18*, 1185.
[31] E. Y. Tiguntseva, Z. Sadrieva, B. V. Stroganov, Y. V. Kapitonov, F. Komissarenko, R. Haroldson, B. Balachandran, W. Hu, Q. Gu, A. A. Zakhidov, A. Bogdanov, S. V. Makarov, *Appl. Surf. Sci.* **2019**, *473*, 419.
[32] A. Y. Zhizhchenko, P. Tonkaev, D. Gets, A. Larin, D. Zuev, S. Starikov, E. V. Pustovalov, A. M. Zakharenko, S. A. Kulinich, S. Juodkazis, A. A. Kuchmizhak, S. V. Makarov, *Small* **2020**, *16*, 2000410.
[33] Y. Lian, L. Jiang, J. Sun, H. Jin, M. Wang, J. Liu, C. Pan, Q. Wang, Z. Chen, *ACS Appl. Mater. Interfaces* **2020**, *12*, 17070.
[34] D. Wu, Z. Zhao, W. Lu, L. Rogée, L. Zeng, P. Lin, Z. Shi, Y. Tian, X. Li, Y. H. Tsang, *Nano Res.* **2021**, *14*, 1973.
[35] D. Wu, J. Guo, C. Wang, X. Ren, Y. Chen, P. Lin, L. Zeng, Z. Shi, X. J. Li, C.-X. Shan, J. Jie, *ACS Nano* **2021**, *15*, 10119.
[36] L. Zeng, D. Wu, J. Jie, X. Ren, X. Hu, S. P. Lau, Y. Chai, Y. H. Tsang, *Adv. Mater.* **2020**, *32*, 2004412.
[37] L. H. Zeng, D. Wu, S. H. Lin, C. Xie, H. Y. Yuan, W. Lu, S. P. Lau, Y. Chai, L. B. Luo, Z. J. Li, *Adv. Funct. Mater.* **2019**, *29*, 1806878.
[38] L. H. Zeng, S. H. Lin, Z. J. Li, Z. X. Zhang, T. F. Zhang, C. Xie, C. H. Mak, Y. Chai, S. P. Lau, L. B. Luo, *Adv. Funct. Mater.* **2018**, *28*, 1705970.
[39] J. Miao, F. Zhang, *Laser Photonics Rev.* **2019**, *13*, 1800204.
[40] M. Liu, J. Wang, K. Yang, Z. Zhao, Z. Zhou, Y. Ma, L. Shen, X. Ma, F. Zhang, *J. Mater. Chem. C* **2021**, *9*, 6357.
[41] Z. Zhao, M. Liu, K. Yang, C. Xu, Y. Guan, X. Ma, J. Wang, F. Zhang, *Adv. Funct. Mater.* **2021**, *31*, 2106009.
[42] W. Li, Y. Xu, J. Peng, R. Li, J. Song, H. Huang, L. Cui, Q. Lin, *ACS Appl. Mater. Interfaces* **2021**, *13*, 2971.
[43] P. Vukusic, J. R. Sambles, C. R. Lawrence, *Nature* **2000**, *404*, 457.

[44] Q. Song, Y. Wang, F. Vogelbacher, Y. Zhan, D. Zhu, Y. Lan, W. Fang, Z. Zhang, L. Jiang, Y. Song, M. Li, *Adv. Energy Mater.* **2021**, *11*, 2100742.
[45] Y. Zhao, Y. Qiu, J. Feng, J. Zhao, G. Chen, H. Gao, Y. Zhao, L. Jiang, Y. Wu, *J. Am. Chem. Soc.* **2021**, *143*, 8437.
[46] Y. Zhao, Y. Qiu, H. Gao, J. Feng, G. Chen, L. Jiang, Y. Wu, *Adv. Mater.* **2020**, *32*, 1905298.
[47] D. Wu, M. Xu, L. Zeng, Z. Shi, Y. Tian, X. J. Li, C.-X. Shan, J. Jie, *ACS Nano* **2022**, *16*, 5545.
[48] L. H. Zeng, Q. M. Chen, Z. X. Zhang, D. Wu, H. Yuan, Y. Y. Li, W. Qarony, S. P. Lau, L. B. Luo, Y. H. Tsang, *Adv. Sci.* **2019**, *6*, 1901134.
[49] D. Wu, J. Guo, J. Du, C. Xia, L. Zeng, Y. Tian, Z. Shi, Y. Tian, X. J. Li, Y. H. Tsang, *ACS Nano* **2019**, *13*, 9907.